RESEARCH ARTICLE

Check for updates

Synthesis of chiral high-entropy sulfides for non-linear optical applications†

Nethmi W. Hewage, [ID] [a,b] Gayatri Viswanathan, [ID] [a,b] Philip Yox, [a,b] Kui Wu, [ID] [c] Kirill Kovnir [ID] *[a,b] and Georgiy Akopov [ID] *[a,b,d]

Non-centrosymmetric semiconductors may exhibit non-linear optical (NLO) properties. For application-relevant materials, a careful balance of high second-harmonic generation (SHG) and high laser damage threshold (LDT) as well as phase-matchability are required. We have previously identified $(A)_2Cu_2Ge_2S_{14}$ (A = Y, La, Sm, and Gd) phases as promising NLO materials. Here, we developed a synthetic method to produce solid solution and high-entropy sulfides containing up to 9 elements. We report the synthesis, crystal structure, and NLO properties for solid solutions and high-entropy multi-metallic materials (HEMs) of the type $(A)_6(TM)_xGe_2S_{14}$ (A = La, Sm, Gd, mixture of (Y + La + Ce + Sm + Gd); TM = Mn, Cu; $1 \leq x \leq 2$). In this work, we establish that nearly all phases are phase matchable and the HEA composition with Cu possesses a SHG signal enhancement of 1.5× as compared to the $AgGaS_2$ (AGS) standard for the largest particle size, as well as a LDT value of 2.8× of AGS.

Introduction

Materials with non-linear optical (NLO) properties are widely used in a range of applications such as medicine, atmospheric sensing, telecommunications materials and biological imaging.[1,2] In order for a material to be suitable for NLO applications, several criteria must be met: the phase has to crystallize in a noncentrosymmetric space group, large crystals or bulk quantities of the material should be readily synthesizable, and lastly the material must possess an appropriate band gap.[3–10] In addition, the material must possess a good balance of high second-harmonic generation (SHG) and high laser damage threshold (LDT), as well as being phase-matchable.

For NLO oxide materials, considerable progress has been made, which can be seen in the plethora of new materials discovered in the past decade: $Pb_{17}O_8Cl_8$,[11] $NaRb_3B_6O_9$,[12] $Sn_2B_5O_9Br$,[13] $Na_4B_8O_9F_{10}$,[14] $CaZn_2(BO_3)_2$,[15] and $Rb_3B_5O_8F_2$.[16]

[a]*Department of Chemistry, Iowa State University, Ames, IA 50011, USA.*
E-mail: kovnir@iastate.edu, georgiy.akopov@rutgers.edu
[b]*Ames National Laboratory, U.S. Department of Energy, Ames, IA 50011, USA*
[c]*State Key Laboratory of Crystal Materials and Institute of Crystal Materials, Shandong University, Jinan, 071002, China*
[d]*Department of Chemistry, Rutgers University – Newark, Newark, NJ 07102, USA*
†Electronic supplementary information (ESI) available: Details of synthesis[21,47–50] and characterization by single and powder X-ray diffraction, scanning electron microscopy and energy dispersive spectroscopy, UV-Vis diffuse reflectance and non-linear optical properties measurements. CCDC 2266451–2266460. For ESI and crystallographic data in CIF or other electronic format see DOI: https://doi.org/10.1039/d3qi01214j

For non-oxide/oxo-halide NLO materials, main progress has been made for chalcogenides: $Li_2Cs_4Ge_2S_5(S_2)Cl_2$,[17] $Zn_2HgP_2S_8$,[18] and $Rb_2CdSi_4S_{10}$.[19]

Among the different chalcogenides, quaternary sulfides of the type $(RE)_6(TM)_x(Z)_2Q_{14}$ (RE = rare-earth; TM = transition metals; Z = Si, Ge, Sn, Be, Fe, Zn, Sm, Yb, B, Al, Ga and In; Q = S and Se) stand out as an extremely large class of compounds which adopt the noncentrosymmetric, chiral, and polar space group $P6_3$.[20–22] Subscript x differs depending on the nature of the Z element and oxidation state of the TM used; for example for Z = Si, x = 2 (Li^+, Cu^+, Au^+), x = 1 (Fe^+, Mn^{2+}), x = 0.67 (Cr^{3+}, Rh^{3+}), and x = 0.5 (Zr^{4+}, Pt^{4+}).[21]

We have previously identified La_3CuGeS_7 ($La_6Cu_2Ge_2S_{14}$) as a potential NLO material with good LDT and SHG properties.[21] Then, following the principle of composition optimization within this prototype structure,[23] we attempted to synthesize phases with better NLO properties by changing La to other rare-earth metals: Y, Ce, Sm, and Gd.[24] Rare-earth cation variation caused changes to the bond lengths and angles of the underlying polyhedral structure. It was determined that Gd_3CuGeS_7 had the best combination of NLO properties with high LDT (3× $AgGaS_2$) and SHG (1.6× $AgGaS_2$ at 88–105 μm particle size) as well as being phase matchable.[24]

In this manuscript, we developed a synthetic method to produce multimetallic solid solution and high entropy phases. We explored the effect of solid-solution formation and high-entropy rare-earth cation mixing on the NLO properties of the resulting multinary sulfides. Solid-solutions between two phases of similar crystal structure are known to be beneficial

This journal is © the Partner Organisations 2023

Inorg. Chem. Front., 2023, **10**, 6613–6621 | **6613**

not only for phase formation, often making the resulting composition more single phase by suppressing the formation of admixture phases, but also by enhancing mechanical (Vickers hardness and incompressibility) and optical properties.[23,25–29] By forming more complex solid solutions, we can achieve the high-entropy alloy (HEA) regime (containing 5 or more elements in a single crystallographic position in the structure). These phases may have additional thermodynamic stabilization owing to contributions from entropy and often have superior properties as compared to their parent non-HEA compounds.[30–33]

Several studies have investigated the effects of solid-solution formation on the resulting NLO properties (mainly SHG). With substitution on the same crystallographic site by atoms with similar characteristics (*e.g.*, charge and polarizability), an enhancement of the SHG signal relative to the standard was observed: $Li_xAg_{1-x}GaSe_2$ ($x = 0.8$, 5× SHG enhancement)[34] and $Al_{5-x}Ga_xBO_9$ ($x \geq 0.4$, 10× SHG enhancement).[35] In cases of solid solution formation with atoms of different polarizability, a decrease in the SHG signal was observed: $Bi_{2-x}RE_xTeO_9$ (RE = Y, Ce and Eu), $Bi_{4-x}La_xTi_3O_{12}$ ($x < 0.75$), $CsBi_{1-x}Eu_xNb_2O_7$ ($x < 2$), $Ca_4Bi_{6-x}Ln_xO_{13}$ (Ln = La and Eu), and $Na_2Mg_{1-x}Zn_xSiO_4$ ($x < 1$).[35] Finally, a decrease of the SHG signal was observed in $Sb^{III}Sb^V_xM_{1-x}O_4$ (M = Nb^V or Ta^V, $x \geq 0.6$), caused by the fact that M^VO_6 octahedra and not the $Sb^{III}O_4E$ unit were mainly responsible for the SHG response.[36]

Herein, we report the synthesis, crystal structures, and NLO properties of several Mn/Cu solid solutions for $(A)_6(TM)Ge_2S_{14}$ (A = La, Sm, Gd, HEA = YLaCeSmGd, TM = Mn, Cu) as well as complex high-entropy alloy compositions, with one having 9 elements (nominal composition of $(YLaCeSmGd)_{1.2}Mn_{0.5}CuGe_2S_{14}$). We have shown the applicability of the method of atomic mixing of refractory components in the synthesis of single-phase homogeneous samples of complex high-entropy sulfides. High entropy materials synthesized in the current work exhibit NLO properties, SHG and LDT, which are on par with the single metal analogs.

Results and discussion

Fig. 1 shows the crystal structure of the mixed metal sulfide $La_6Mn_{0.5}CuGe_2S_{14}$. Detailed crystallographic information can be seen in Tables S1A and S1B.† This phase crystallizes in the noncentrosymmetric, chiral, and polar space group $P6_3$, making it a good candidate for non-linear optical (NLO) materials.[21,37,38] The crystal structure is composed of several types of space-filling polyhedra.[21,22,24] In analogy with the structures of the solid solution end members (containing only one transition metal), in the crystal structure of $La_6Mn_{0.5}CuGe_2S_{14}$, Mn and Cu occupy two distinct positions in face-sharing S_6 octahedra. Mn^{2+} atoms occupy the centers of the octahedra, forming $[MnS_6]$ units, while Cu^+ occupies the opposite faces of the octahedra, forming $[CuS_3]$ trigonal planes (Fig. 1b and c). For a 50/50% solid solution, the octahedra will be occupied either by the Mn atom in the center or the Cu atoms on the faces, giving a "$Mn_{0.5}Cu$" composition. The tetrel atom, Ge, forms $[GeS_4]$ tetrahedra, which fill the space around $[LaS_8]$ units. The Ge1–S1 bond is shorter than the other three Ge–S bonds and points along the [001] direction (*c*-axis) (Fig. 1d and Tables S2A–C†). The lanthanide, in this case La, forms $[LaS_8]$ dodecahedra, which arrange in spiral columns (Fig. 1e).

The synthesis of high-entropy alloys is a challenge,[39–42] and the synthesis of sulfides is complicated by the high vapor pressure of sulfur at elevated temperatures. For synthesis from elements or binary sulfides for multi-metal phases, it is difficult to achieve proper mixing and distribution of metals. Our solution was to use the method of atomic mixing of the
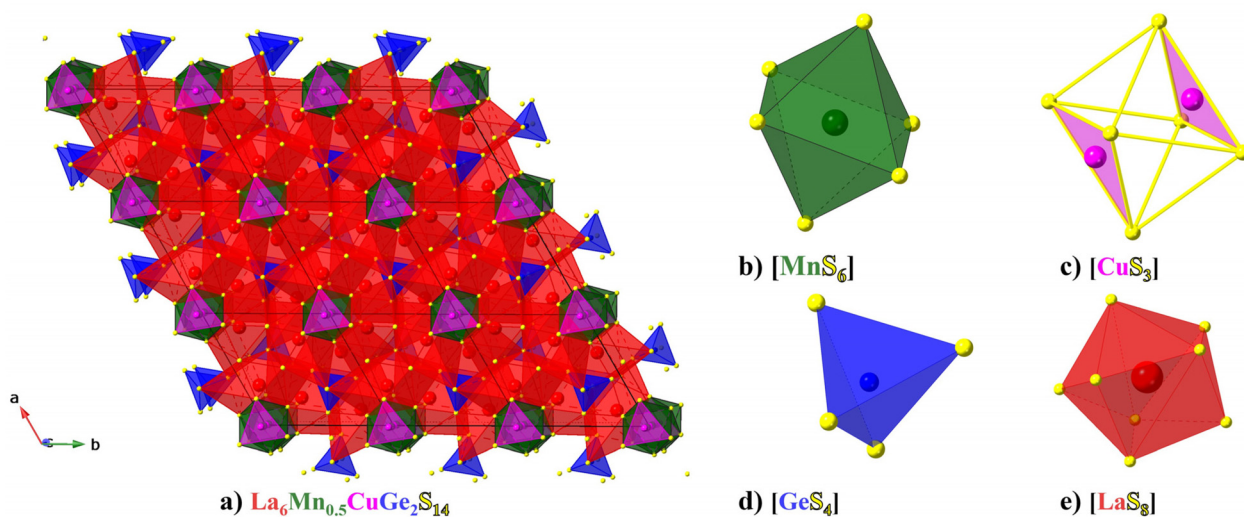

Fig. 1 (a) Crystal structure of $La_6Mn_{0.5}CuGe_2S_{14}$ ($P6_3$, no. 173) showing the connectivity of polyhedra; (b) green $[MnS_6]$ octahedron; (c) pink $[CuS_3]$ trigonal planes shown occupying opposite faces of a hypothetical octahedron; (d) blue $[GeS_4]$ tetrahedron; and (e) red $[LaS_8]$ dodecahedron.

6614 | *Inorg. Chem. Front.*, 2023, **10**, 6613–6621

This journal is © the Partner Organisations 2023

refractory components.[12,31] By reacting homogenized arc-melted precursors of the nominal composition $(A)_6(TM)Ge_2$ with sulfur, we can achieve significantly better atomic mixing and produce bulk powder samples with high enough purity and homogeneity to be suitable for NLO measurements, as well as grow large single crystals (see the ESI† for details). This method was used to produce Mn/Cu solid solution phases for La, Sm and Gd, as well as the high-entropy alloy (Y + La + Ce + Sm + Gd) phases for Mn, Cu and Mn/Cu – the last having 9 elements in the composition.

The powder X-ray diffraction (PXRD) data for the synthesized phases are shown in Fig. 2. The common feature is that the compositions with only Mn often have secondary admixture phases (which can affect the optical properties), while compositions with Cu or mixed Mn/Cu systems are in single-phase. The high-entropy alloy (HEA) composition phases, including the nonary $(YLaCeSmGd)_{1.2}Mn_{0.5}CuGe_2S_{14}$ sample, show very clean powder patterns without substantial peak broadening, suggesting a homogeneous single-phase product, which can be ascribed to the favorable nature of solid-solution and HEA formation for a given system.

Elemental compositions were verified using energy dispersive spectroscopy (EDS), which showed good agreement of the nominal and EDS compositions, even for the high-entropy alloy compositions (Tables 1 and 2). Deviations from the nominal compositions can be attributed to the fact that the emission lines for the lanthanides, Cu, and Ge have partial overlap. The atomic percentage of light elements, sulfur in this case, is often underestimated by EDS. HEA materials with Cu and Mn/Cu show good agreement between the nominal and actual contents of rare-earth (RE) metals (Table 2). In turn, HEA materials with Mn only, in line with the observed broad and split peaks in the PXRD pattern, have a rare-earth metal content which is different from the nominal content (Y-poor and Ce-rich).

A suitable band gap is another crucial requirement for infrared (IR) NLO materials. The Tauc plots for the $(A)_6(TM)Ge_2S_{14}$ samples are shown in Fig. 3. Optical images of the crystals of the sulfides can be seen in Fig. S1.† All compositions are semiconducting phases with visible range direct bandgaps of 1.75–2.31 eV, which are slightly smaller than the bandgap of the standard $AgGaS_2$ (2.5 eV).[22] The insets in Fig. 3 show the optical images of the powders for these sulfide phases. It can
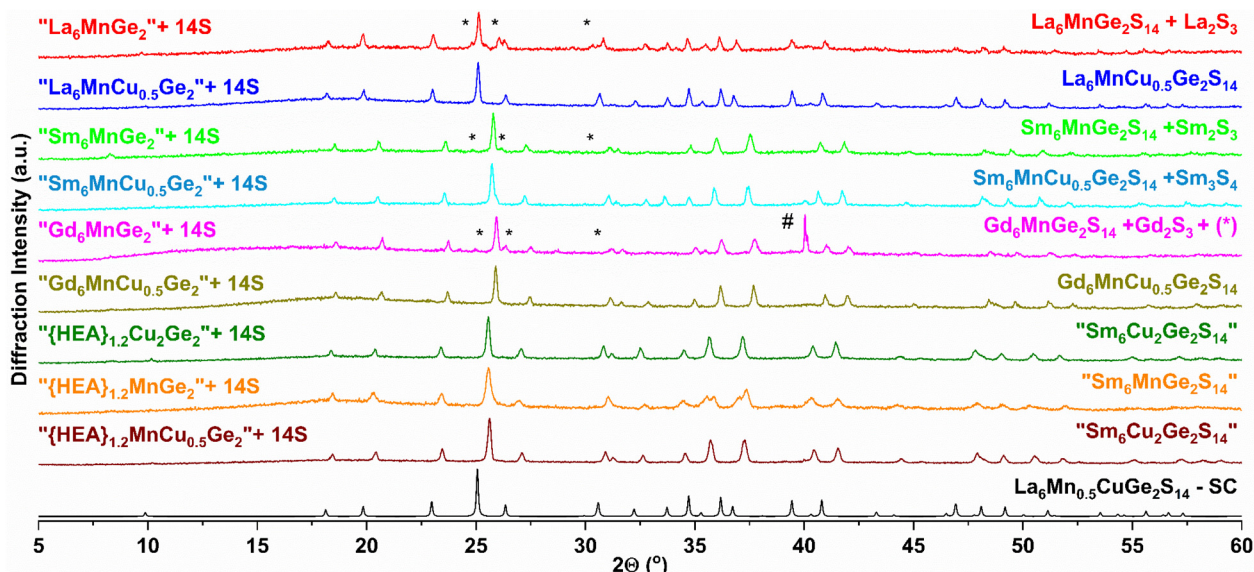

Fig. 2 PXRD data for the phase formation of the $(A)_6(TM)Ge_2S_{14}$ compositions (A = La, Sm, Gd, HEA = YLaCeSmGd, TM = Mn, Cu). Nominal compositions are given in quotation marks (" "). The pattern in black is calculated from the single crystal (SC) structural solution. Diffraction peaks corresponding to admixtures are labeled as (*) and re-crystallized grease as (#).

Table 1 EDS compositions for powder samples of $(A)_6(TM)Ge_2S_{14}$ composition (A = La, Sm, Gd, TM = Mn, Cu) phases when normalized to 6 A atoms. For each sample, 10–20 sites were probed and averaged to determine the average composition. Standard deviations are given in parentheses. To test the reproducibility, two different synthesized batches of samples were studied

Nominal composition	EDS composition from batch 1	EDS composition from batch 2
$La_6MnGe_2S_{14}$	$La_6Mn_{0.93(6)}Ge_{2.12(11)}S_{12.6(4)}$	$La_6Mn_{0.94(3)}Ge_{2.1(1)}S_{12.8(2)}$
$La_6Mn_{0.5}CuGe_2S_{14}$	$La_6Mn_{0.53(3)}Cu_{1.0(1)}Ge_{1.78(3)}S_{13.14(5)}$	$La_6Mn_{0.53(2)}Cu_{0.94(5)}Ge_{1.77(4)}S_{13.09(7)}$
$Sm_6MnGe_2S_{14}$	$Sm_6Mn_{0.7(1)}Ge_{1.94(9)}S_{13.1(2)}$	$Sm_6Mn_{0.71(9)}Ge_{1.94(4)}S_{12.9(1)}$
$Sm_6Mn_{0.5}CuGe_2S_{14}$	$Sm_6Mn_{0.30(5)}Cu_{1.4(1)}Ge_{2.00(9)}S_{13.17(2)}$	$Sm_6Mn_{0.29(4)}Cu_{1.4(1)}Ge_{1.9(2)}S_{13.1(1)}$
$Gd_6MnGe_2S_{14}$	$Gd_6Mn_{0.81(6)}Ge_{2.0(2)}S_{13.27(9)}$	$Gd_6Mn_{0.77(6)}Ge_{2.0(2)}S_{13.2(2)}$
$Gd_6Mn_{0.5}CuGe_2S_{14}$	$Gd_6Mn_{0.40(5)}Cu_{1.09(5)}Ge_{1.20(7)}S_{13.6(2)}$	$Gd_6Mn_{0.38(5)}Cu_{0.9(2)}Ge_{1.1(2)}S_{13.7(1)}$

This journal is © the Partner Organisations 2023

Inorg. Chem. Front., 2023, **10**, 6613–6621 | **6615**

Table 2 EDS compositions for powder samples of $(HEA)_6(TM)Ge_2S_{14}$ composition (HEA = YLaCeSmGd, TM = Mn, Cu) phases when normalized to 6 HEA atoms. For each of the three compositions, the high-entropy composition is given in the second row. For each sample, 10−20 sites were probed and averaged to determine the average composition. Standard deviation is given in parentheses. To test the reproducibility, two different synthesized batches of samples were studied

Nominal composition	EDS composition from batch 1	EDS composition from batch 2
$(YLaCeSmGd)_{1.2}Cu_2Ge_2S_{14}$	$(HEA1)_6Cu_{1.87(4)}Ge_{1.83(6)}S_{13.1(1)}$	$(HEA1)_6Cu_{1.83(6)}Ge_{1.8(1)}S_{12.9(2)}$
HEA1	$Y_{1.1(1)}La_{1.4(2)}Ce_{1.1(2)}Sm_{1.3(2)}Gd_{1.1(2)}$	$Y_{1.2(2)}La_{1.3(3)}Ce_{1.1(2)}Sm_{1.3(3)}Gd_{1.1(2)}$
$(YLaCeSmGd)_{1.2}MnGe_2S_{14}$	$(HEA2)_6Mn_{0.93(4)}Ge_{1.70(6)}S_{12.8(2)}$	$(HEA2)_6Mn_{0.93(3)}Ge_{1.74(7)}S_{12.9(2)}$
HEA2	$Y_{0.5(1)}La_{1.1(3)}Ce_{2.2(3)}Sm_{1.3(2)}Gd_{0.8(4)}$	$Y_{0.6(1)}La_{1.0(2)}Ce_{2.2(3)}Sm_{1.5(2)}Gd_{0.71(8)}$
$(YLaCeSmGd)_{1.2}Mn_{0.5}CuGe_2S_{14}$	$(HEA3)_6Mn_{0.43(3)}Cu_{1.10(5)}Ge_{1.74(9)}S_{13.1(2)}$	$(HEA3)_6Mn_{0.37(4)}Cu_{1.07(5)}Ge_{1.78(8)}S_{13.2(2)}$
HEA3	$Y_{1.18(9)}La_{1.2(1)}Ce_{1.25(6)}Sm_{1.14(7)}Gd_{1.19(7)}$	$Y_{1.13(9)}La_{1.3(2)}Ce_{1.27(4)}Sm_{1.13(8)}Gd_{1.13(7)}$

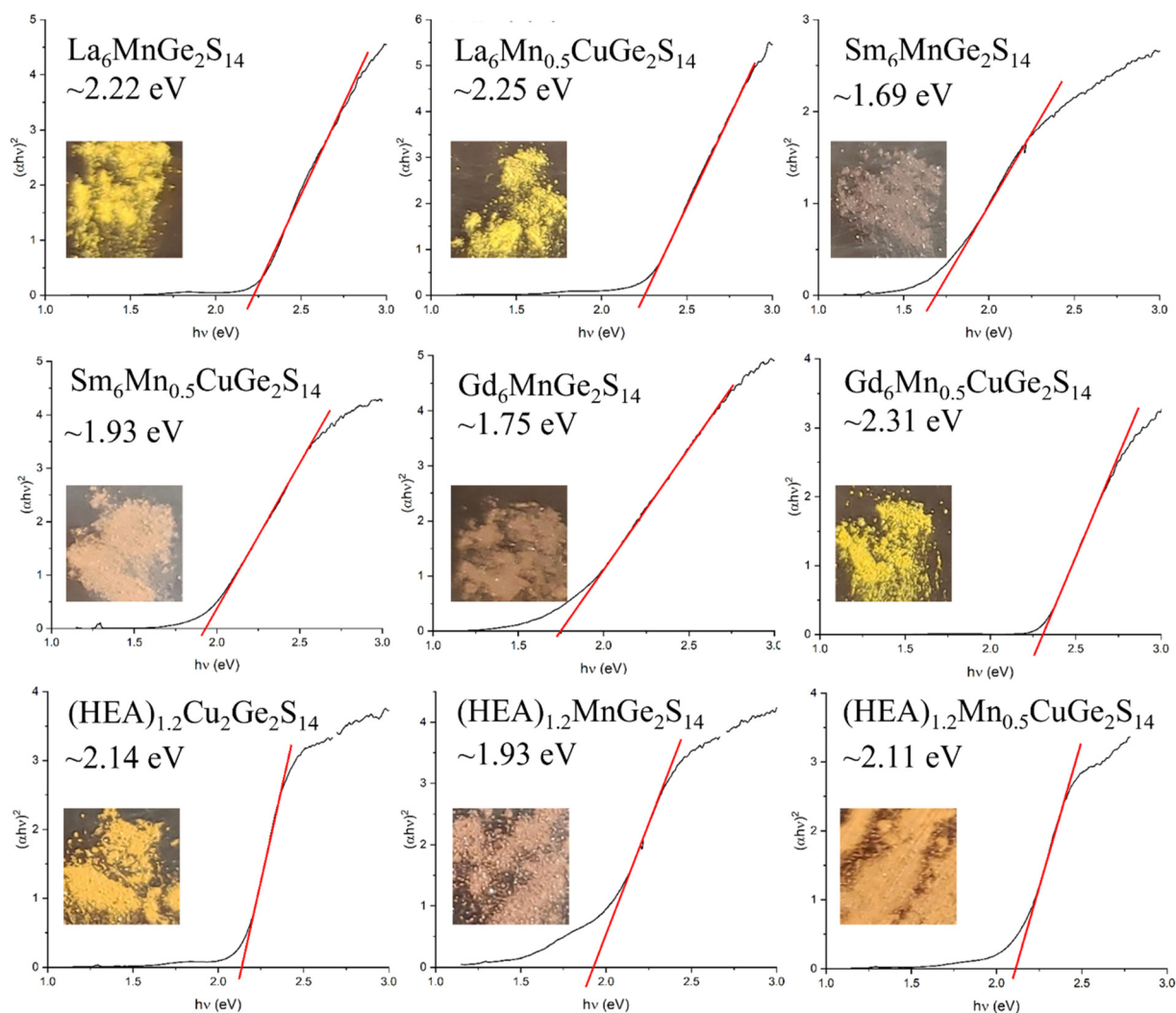**Fig. 3** Tauc plots showing direct band gaps $(\alpha h\nu)^2$ for the $(A)_6(TM)Ge_2S_{14}$ compositions (A = La, Sm, Gd, HEA = YLaCeSmGd, TM = Mn, Cu) measured using diffuse reflectance UV-Vis spectroscopy. Insets: optical images of powdered samples showing the colors of the phases.

be noted that compositions with Mn are more red-brown in color (which could be due to the presence of a small amount of admixture phases), while the compositions with Cu or Mn/Cu are more yellow. We have previously reported $(RE)_6CuGe_2S_{14}$ compositions with good NLO properties, having larger band gaps of 2.1–2.7 eV.[24] However, another member of

the same sulfide family, $La_6PdSi_2S_{14}$, possesses very good NLO properties while having a much smaller band gap of 1.4 eV.[22] $IrSi_3As_3$ is another example of a compound with a smaller band gap and good NLO properties.[43]

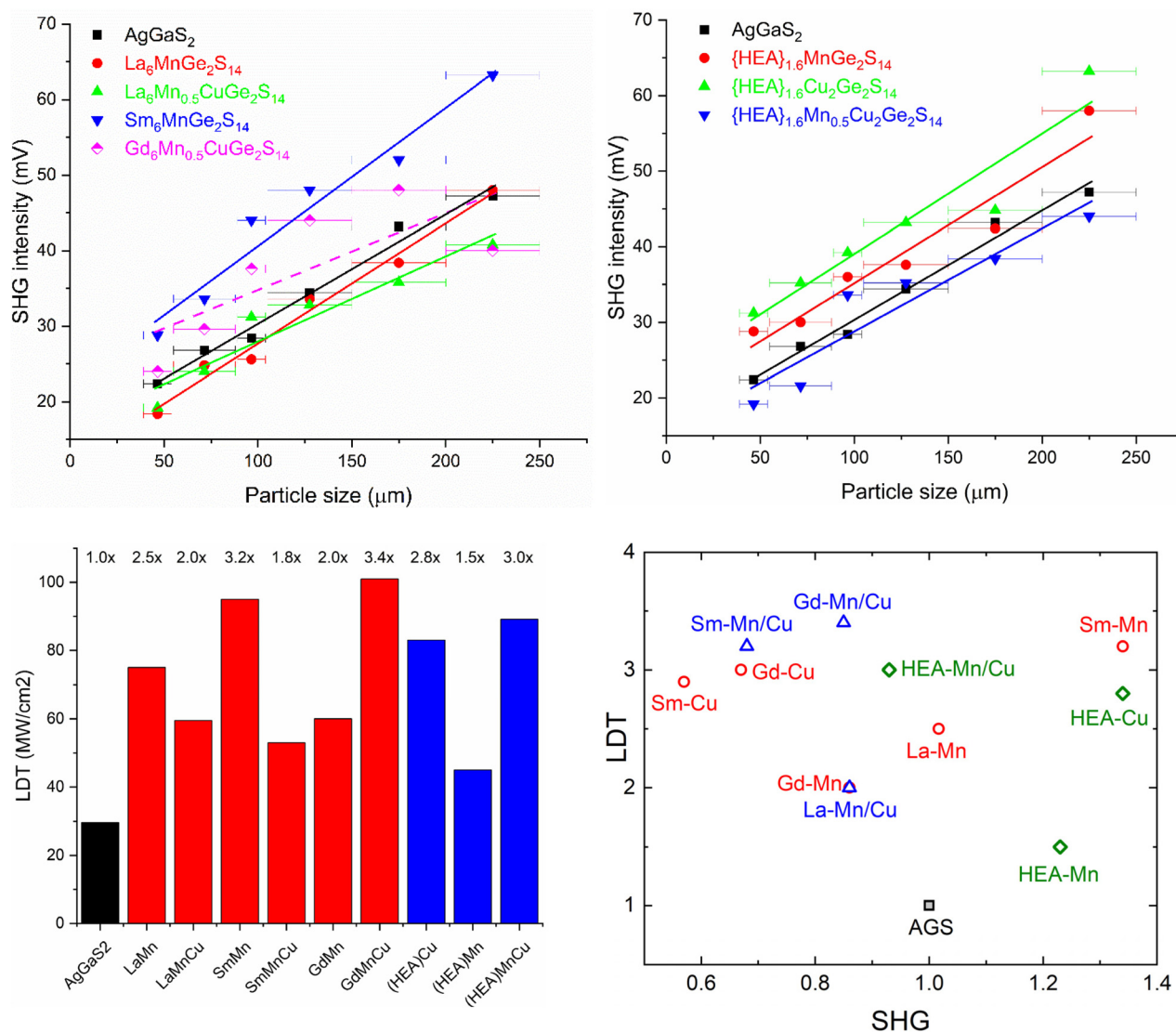The second-harmonic generation (SHG) signal data for these phases are shown in Fig. 4 (top and middle) and

Fig. 4 (Top) Second-harmonic generation (SHG) intensity for $(A)_6(TM)Ge_2S_{14}$ compositions (A = La, Sm, Gd, HEA = YLaCeSmGd, TM = Mn, Cu). The solid lines are drawn to guide the eye. All compositions are phase matchable except $Gd_6Mn_{0.5}CuGe_2S_{14}$ (shown with a dashed pink line). (Bottom Left) Laser damage threshold (LDT) intensities for $(A)_6(TM)Ge_2S_{14}$ compositions. Numbers above the columns indicate the value of LDT relative to the standard $AgGaS_2$. Standard $AgGaS_2$ is shown in black in all panels. (Bottom right) SHG/LDT diagram showing SHG values at the maximum studied particle size and LDT values normalized to those for the AGS standard. Data for single RE−Cu compositions are taken from ref. 24.

Table S3.† The compositions with pure Mn contain admixtures which have an effect on the NLO properties measured. All the compositions analyzed (except for $Gd_6Mn_{0.5}CuGe_2S_{14}$), including the HEAs, are phase matchable, which means that they show an increase in the SHG signal with increasing particle size. This is very important for NLO applications as it signifies that the bulk material possesses good NLO properties.

The SHG signals for the largest particle size (200–250 μm) are comparable or better than those of the AgGaS₂ standard, with the two HEA compositions having values of almost 1.5 times the standard (Fig. 4). All compositions show an enhancement of LDT over the AgGaS₂ standard with values ranging from 1.5× to 3.4×. The trends shown in the Fig. 4 bottom right panel allow us to compare HEA compositions with single RE

compositions. For the cases of TM = Mn no clear trends are obtained which may be partially due to the non-single phase nature of the samples. However, for TM = Cu or Cu/Mn there is a clear trend that HEA mixing of the rare-earth cations enhances the SHG response while only slightly decreasing LDT, suggesting that this technique may be a viable strategy to enhance the NLO performance in reported materials.[44,45]

To understand the trends in the NLO data, it is important to analyze the bonding within and between the different polyhedral units (Tables S2A–C† and Fig. 5). As expected, the unit cell volumes decrease for both Mn and Cu end members going from La to Gd (Mn: from 539.77 to 488.54 Å³, Cu: from 537.95 to 493.07 Å³)[24] because the size of the lanthanide decreases.[46] The HEA compositions have unit cell volumes between those
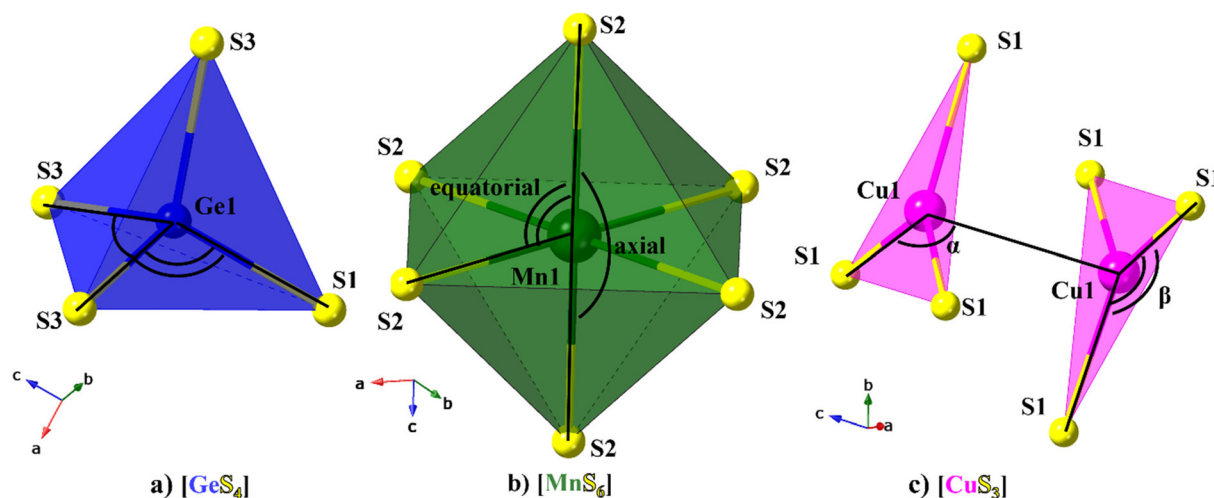
This journal is © the Partner Organisations 2023

Inorg. Chem. Front., 2023, **10**, 6613–6621 | **6617**

Fig. 5 (a) [GeS₄] tetrahedral unit showing ∠S3–Ge–S1 and ∠S3–Ge1–S3 angles; (b) [MnS₆] octahedral unit showing ∠S2–Mn–S2-axial and ∠S2–Mn1–S2-equatorial angles; (c) two [CuS₃] trigonal planar units showing angle α (∠Cu1–Cu1–S2) indicating the co-planarity of these two units (perfect co-planarity having α = 90°), and angle β (∠S2–Cu1–S2) indicating the deviation from the planar D_{3h} ($\bar{6}m2$) symmetry for [CuS₃] (in planar β = 120°).

of the pure lanthanide parent phases (514.70–521.19 Å³). For the dodecahedral [(RE)S₈] units, the polyhedral volumes (46.97–42.13 Å³) and the mean RE–S bond lengths (3.004–2.899 Å) decrease going from La to Gd, as expected. There is no obvious correlation between the rare-earth and [GeS₄] tetrahedron volume (~5.5 Å³) or Ge–S bond lengths (mean lengths: ~2.21 Å). However, the Ge1–S1 bond length is noticeably shorter than the Ge1–S3 bond length in all cases, leading to a local C_{3v} ($3mm$) symmetry, with the greatest difference in bond lengths observed in the case of Gd and HEA compositions with Mn. This in turn causes the S–Ge–S angles to deviate from the ideal 109.5° angle (Fig. 5a).

For the octahedral [MnS₆] units, the polyhedral volumes (26.05–23.76 Å³) and Mn–S mean bond length (2.698–2.615 Å) somewhat follow a similar trend – both decrease upon going from La to Gd. The axial S2–Mn1–S2 angles (Fig. 5b) are all very close to 180°; however the equatorial angles (86.559–87.032°) differ from the ideal 90° showing that the octahedra are slightly distorted. Finally, for the trigonal planar [CuS₃] units (Fig. 5c), the Cu–S bonds (2.269–2.222 Å) decrease going from La to Gd as expected. In all cases, the [CuS₃] units lack coplanarity as is evident from the values of angle α (88.391–92.351°) which deviates from the ideal 90°. At the same time, within each CuS₃ unit, atoms are nearly planar as is evident from the β angles (119.833–119.898°) being close to 120°. Comparing the data for RE–Cu compositions[24] and (HEA)–Cu, as well as RE–Mn with (HEA)–Mn, it can be noted that the formation of HEAs does not seem to induce additional significant long range distortions. However, it is possible that alternation of larger and smaller rare-earth cations may induce local perturbations which affect the SHG and LDT properties. Further studies using X-ray total scattering and EXAFS will be required to clarify these local distortions.

In summary, it can be shown that LDT and SHG responses have different trends with respect to TM solid solution formation. The mixing of Mn and Cu was beneficial for enhancing LDT relative to not only the standard AgGaS₂, but also most of their single transition metal counterparts. LDT enhancement can be attributed to the added crystallographic disorder due to Mn and Cu partially occupying different crystallographic positions in the structure (Mn at the center of the octahedron, while Cu being on the faces of the octahedron) (Fig. 1), as well as the stability and relatively small anisotropy of the Ge–S bonds in [GeS₄] tetrahedral units (which can be seen from a 2.02–2.39% bond length difference, Table S2†). This is similar to the decrease of the SHG signal observed in $Sb^{III}Sb_x^V M_{1-x}O_4$ (M = Nb^V or Ta^V, $x \geq 0.6$), caused by the fact that $M^V O_6$ octahedra are mainly responsible for the SHG effect.[36] In turn, HEA phases with multiple rare-earth cations show performance on par or better than the corresponding single RE compounds. Analyses of the crystal structures do not reveal any special long-range structural deformations for HEA compounds, yet one can assume that the optimization of chemical bonding may occur on the local scale. These results together, along with the reported method of synthesis for complex HEA sulfides, open ways to use mixtures of rare-earth metals (such as mischmetal), rather than purified single RE metals, to synthesize efficient NLO compounds with properties benefiting from the high-entropy nature of the materials.

Conclusions

The effects of structural peculiarities on NLO properties are a complex problem. To analyze the effect of solid-solutions and structural entropy on NLO properties, several compositions

6618 | *Inorg. Chem. Front.*, 2023, **10**, 6613–6621

This journal is © the Partner Organisations 2023

within the $(A)_6(TM)_xGe_2S_{14}$ family of compounds (A = La, Sm, Gd, HEA = YLaCeSmGd, TM = Mn, Cu) were synthesized by a simple reaction of arc-melted precursors with elemental sulfur. The compositions resembling those of Mn/Cu solid solutions or HEAs not only showed SHG signals comparable to or better than the AgGaS$_2$ standard but are also phase matchable and show an enhancement of LDT relative to the standard. The best NLO properties were achieved for the HEA compound $(YLaCeSmGd)_{1.2}Cu_2Ge_2S_{14}$, showing an SHG enhancement of almost 1.5× AgGaS$_2$ at the largest particle size (200–250 μm), together with an LDT enhancement of 2.8× the standard.

Conflicts of interest

There are no conflicts to declare.

Acknowledgements

References

1 D. N. Nikogosyan, *Nonlinear Optical Crystals: A Complete Survey*, Springer-Science, New York, 2005.

2 R. W. Boyd, *Nonlinear Optics*, Elsevier Science, 3rd edn, 2008.

3 V. Petrov, Progress in 1-Mm Pumped Mid-IR Optical Parametric Oscillators Based on Non-Oxide Nonlinear Crystals, *IEEE J. Sel. Top. Quantum Electron.*, 2015, **21**(1), 193–206, DOI: **10.1109/JSTQE.2014.2378595**.

4 V. Petrov, Frequency Down-Conversion of Solid-State Laser Sources to the Mid-Infrared Spectral Range Using Non-Oxide Nonlinear Crystals, *Prog. Quantum Electron.*, 2015, **42**, 1–106, DOI: **10.1016/j.pquantelec.2015.04.001**.

5 L. I. Isaenko and A. P. Yelisseyev, Recent Studies of Nonlinear Chalcogenide Crystals for the Mid-IR, *Semicond. Sci. Technol.*, 2016, **31**(12), 123001, DOI: **10.1088/0268-1242/31/12/123001**.

6 M. Mutailipu, K. R. Poeppelmeier and S. Pan, Borates: A Rich Source for Optical Materials, *Chem. Rev.*, 2021, **121**(3), 1130–1202, DOI: **10.1021/acs.chemrev.0c00796**.

7 J. Chen, C. Lin, D. Zhao, M. Luo, G. Peng, B. Li, S. Yang, Y. Sun and N. Ye, Anionic Aliovalent Substitution from Structure Models of ZnS: Novel Defect Diamond–like Halopnictide Infrared Nonlinear Optical Materials with Wide Band Gaps and Large SHG Effects, *Angew. Chem., Int. Ed.*, 2020, **59**(52), 23549–23553, DOI: **10.1002/anie.202010319**.

8 G. Li, K. Wu, Q. Liu, Z. Yang and S. Pan, Na$_2$ZnGe$_2$S$_6$: A New Infrared Nonlinear Optical Material with Good Balance between Large Second-Harmonic Generation Response and High Laser Damage Threshold, *J. Am. Chem. Soc.*, 2016, **138**(23), 7422–7428, DOI: **10.1021/jacs.6b03734**.

9 S.-F. Li, X.-M. Jiang, Y.-H. Fan, B.-W. Liu, H.-Y. Zeng and G.-C. Guo, New Strategy for Designing Promising Mid-Infrared Nonlinear Optical Materials: Narrowing the Band Gap for Large Nonlinear Optical Efficiencies and Reducing the Thermal Effect for a High Laser-Induced Damage Threshold, *Chem. Sci.*, 2018, **9**(26), 5700–5708, DOI: **10.1039/C8SC01210E**.

10 K. Wu, Y. Chu, Z. Yang and S. Pan, A$_2$SrMIVS$_4$ (A = Li, Na; MIV = Ge, Sn) Concurrently Exhibiting Wide Bandgaps and Good Nonlinear Optical Responses as New Potential Infrared Nonlinear Optical Materials, *Chem. Sci.*, 2019, **10**(14), 3963–3968, DOI: **10.1039/C9SC00028C**.

11 H. Zhang, M. Zhang, S. Pan, X. Dong, Z. Yang, X. Hou, Z. Wang, K. B. Chang and K. R. Poeppelmeier, Pb$_{17}$O$_8$Cl$_{18}$: A Promising IR Nonlinear Optical Material with Large Laser Damage Threshold Synthesized in an Open System, *J. Am. Chem. Soc.*, 2015, **137**(26), 8360–8363, DOI: **10.1021/jacs.5b03986**.

12 F. Ding, W. Zhang, M. L. Nisbet, W. Zhang, P. S. Halasyamani, Z. Yang, S. Pan and K. R. Poeppelmeier, NaRb$_3$B$_6$O$_9$(OH)$_3$(HCO$_3$): A Borate-Bicarbonate Nonlinear Optical Material, *Inorg. Chem.*, 2020, **59**(1), 759–766, DOI: **10.1021/acs.inorgchem.9b03026**.

13 J. Guo, S. Cheng, S. Han, Z. Yang and S. Pan, Sn$_2$B$_5$O$_9$ Br as an Outstanding Bifunctional Material with Strong Second–Harmonic Generation Effect and Large Birefringence, *Adv. Opt. Mater.*, 2021, **9**(5), 2001734, DOI: **10.1002/adom.202001734**.

14 H. Cheng, F. Li, Z. Yang and S. Pan, Na$_4$B$_8$O$_9$F$_{10}$: A Deep–Ultraviolet Transparent Nonlinear Optical Fluorooxoborate with Unexpected Short Phase–Matching Wavelength Induced by Optimized Chromatic Dispersion, *Angew. Chem., Int. Ed.*, 2022, **61**(10), e202115669, DOI: **10.1002/anie.202115669**.

15 M. Mutailipu, F. Li, C. Jin, Z. Yang, K. R. Poeppelmeier and S. Pan, Strong Nonlinearity Induced by Coaxial Alignment of Polar Chain and Dense [BO$_3$] Units in CaZn$_2$(BO$_3$)$_2$, *Angew. Chem., Int. Ed.*, 2022, **61**(21), e202202096, DOI: **10.1002/anie.202202096**.

16 R. Zhang, B. Cheng, X. Wang, R. Yang, Z. Yang, S. Han and S. Pan, Rb$_3$B$_5$O$_8$F$_2$ and K$_{0.6}$Rb$_{2.4}$B$_5$O$_8$F$_2$: Two New Deep-

This journal is © the Partner Organisations 2023

Inorg. Chem. Front., 2023, **10**, 6613–6621 | **6619**

Ultraviolet Transparent Nonlinear Optical Fluorooxoborates Designed by Cation Regulation, *Inorg. Chem. Front.*, 2023, **10**(3), 787–792, DOI: **10.1039/D2QI01466A**.

17 G. Li, K. Wu, Y. Huang, Z. Yang and S. Pan, $[Ge_2S_5(S_2)]_4^-$, A NLO–Active Unit Leading to an Asymmetric Structure Discovered in $Li_2Cs_4Ge_2S_5(S_2)Cl_2$: An Experimental and Theoretical Study, *Chem. – Eur. J.*, 2019, **25**(21), 5440–5444, DOI: **10.1002/chem.201901012**.

18 Y. Chu, H. Wang, T. Abutukadi, Z. Li, M. Mutailipu, X. Su, Z. Yang, J. Li and S. Pan, $Zn_2HgP_2S_8$: A Wide Bandgap Hg–Based Infrared Nonlinear Optical Material with Large Second–Harmonic Generation Response, *Small*, 2023, 2305074, DOI: **10.1002/smll.202305074**.

19 J. Zhou, Z. Fan, K. Zhang, Z. Yang, S. Pan and J. Li, $Rb_2CdSi_4S_{10}$: Novel $[Si_4S_{10}]$ T_2-Supertetrahedra-Contained Infrared Nonlinear Optical Material with Large Band Gap, *Mater. Horiz.*, 2023, **10**(2), 619–624, DOI: **10.1039/D2MH01200F**.

20 Z. Ye, S. Bardelli, K. Wu, A. Sarkar, A. Swindle and J. Wang, Synthesis, Crystal Growth, Electronic Properties and Optical Properties of $Y_6IV_{2.5}S_{14}$ (IV=Si, Ge), *Z. Anorg. Allg. Chem.*, 2021, e202100271, DOI: **10.1002/zaac.202100271**.

21 G. Akopov, N. W. Hewage, P. Yox, G. Viswanathan, S. J. Lee, L. P. Hulsebosch, S. D. Cady, A. L. Paterson, F. A. Perras, W. Xu, K. Wu, Y. Mudryk and K. Kovnir, Synthesis-Enabled Exploration of Chiral and Polar Multivalent Quaternary Sulfides, *Chem. Sci.*, 2021, **12**, 14718–14730, DOI: **10.1039/D1SC03685H**.

22 G. Akopov, G. Viswanathan, N. W. Hewage, P. Yox, K. Wu and K. Kovnir, Pd and Octahedra Do Not Get along: Square Planar $[PdS_4]$ Units in Non-Centrosymmetric $La_6PdSi_2S_{14}$, *J. Alloys Compd.*, 2022, **902**, 163756, DOI: **10.1016/j.jallcom.2022.163756**.

23 L. Gao, X. Wu, J. Xu, X. Tian, B. Zhang and K. Wu, Rational Combination of Multiple Structural Groups on Regulating Nonlinear Optical Property in Hexagonal Ln_3MGeS_7 Polar Crystals, *J. Alloys Compd.*, 2022, **900**, 163535, DOI: **10.1016/j.jallcom.2021.163535**.

24 G. Akopov, N. W. Hewage, G. Viswanathan, P. Yox, K. Wu and K. Kovnir, Non–Linear Optical Properties of the $(RE)_3CuGeS_7$ Family of Compounds, *Z. Anorg. Allg. Chem.*, 2022, **648**(15), DOI: **10.1002/zaac.202200096**.

25 G. Akopov, M. T. Yeung, Z. C. Sobell, C. L. Turner, C.-W. Lin and R. B. Kaner, Superhard Mixed Transition Metal Dodecaborides, *Chem. Mater.*, 2016, **28**(18), 6605–6612, DOI: **10.1021/acs.chemmater.6b02632**.

26 G. Akopov, W. H. Mak, D. Koumoulis, H. Yin, B. Owens-Baird, M. T. Yeung, M. H. Muni, S. Lee, I. Roh, Z. C. Sobell, P. L. Diaconescu, R. Mohammadi, K. Kovnir and R. B. Kaner, Synthesis and Characterization of Single-Phase Metal Dodecaboride Solid Solutions: $Zr_{1-x}Y_xB_{12}$ and $Zr_{1-x}U_xB_{12}$, *J. Am. Chem. Soc.*, 2019, **141**(22), 9047–9062, DOI: **10.1021/jacs.9b03482**.

27 J. Lei, G. Akopov, M. T. Yeung, J. Yan, R. B. Kaner and S. H. Tolbert, Radial X–Ray Diffraction Study of Superhard

28 Early Transition Metal Dodecaborides under High Pressure, *Adv. Funct. Mater.*, 2019, **29**(22), 1900293, DOI: **10.1002/adfm.201900293**.

28 J. Zhou, L. Luo, Y. Chu, P. Wang, Z. Guo, X. Su and J. Li, Partial Congener Substitution Induced Centrosymmetric to Noncentrosymmetric Structural Transformation and Nonlinear Optical Properties of $PbSnSiS_4$, *J. Alloys Compd.*, 2022, **899**, 163366, DOI: **10.1016/j.jallcom.2021.163366**.

29 S. Balijapelly, A. J. Craig, J. Bin Cho, J. I. Jang, K. Ghosh, J. A. Aitken, A. V. Chernatynskiy and A. Choudhury, Building-Block Approach to the Discovery of $Na_8Mn_2(Ge_2Se_6)_2$: A Polar Chalcogenide Exhibiting Promising Harmonic Generation Signals with a High Laser-Induced Damage Threshold, *J. Alloys Compd.*, 2022, **900**, 163392, DOI: **10.1016/j.jallcom.2021.163392**.

30 D. Wu, K. Kusada, Y. Nanba, M. Koyama, T. Yamamoto, T. Toriyama, S. Matsumura, O. Seo, I. Gueye, J. Kim, L. S. Rosantha Kumara, O. Sakata, S. Kawaguchi, Y. Kubota and H. Kitagawa, Noble-Metal High-Entropy-Alloy Nanoparticles: Atomic-Level Insight into the Electronic Structure, *J. Am. Chem. Soc.*, 2022, **144**(8), 3365–3369, DOI: **10.1021/jacs.1c13616**.

31 C. M. Rost, E. Sachet, T. Borman, A. Moballegh, E. C. Dickey, D. Hou, J. L. Jones, S. Curtarolo and J.-P. Maria, Entropy-Stabilized Oxides, *Nat. Commun.*, 2015, **6**(1), 8485, DOI: **10.1038/ncomms9485**.

32 A. Sarkar, C. Loho, L. Velasco, T. Thomas, S. S. Bhattacharya, H. Hahn and R. Djenadic, Multicomponent Equiatomic Rare Earth Oxides with a Narrow Band Gap and Associated Praseodymium Multivalency, *Dalton Trans.*, 2017, **46**(36), 12167–12176, DOI: **10.1039/C7DT02077E**.

33 A. Sarkar, B. Eggert, L. Velasco, X. Mu, J. Lill, K. Ollefs, S. S. Bhattacharya, H. Wende, R. Kruk, R. A. Brand and H. Hahn, Role of Intermediate 4f States in Tuning the Band Structure of High Entropy Oxides, *APL Mater.*, 2020, **8**(5), 051111, DOI: **10.1063/5.0007944**.

34 J. Peng, X. Liu, J. Wang, S. Zhang, X. Xiao, Z. Xiong, K. Zhang, B. Chen, Z. He and W. Huang, Crystal Growth, Characterization, and Properties of Nonlinear Optical Crystals of $LixAg_{1-x}GaSe_2$ for Mid-Infrared Applications, *Inorg. Chem.*, 2023, **62**(30), 12067–12078, DOI: **10.1021/acs.inorgchem.3c01582**.

35 H. Jo, S.-J. Oh and K. M. Ok, Noncentrosymmetric (NCS) Solid Solutions: Elucidating the Structure–Nonlinear Optical (NLO) Property Relationship and Beyond, *Dalton Trans.*, 2017, **46**(45), 15628–15635, DOI: **10.1039/C7DT02960H**.

36 K. M. Ok, N. S. P. Bhuvanesh and P. S. Halasyamani, $SbSbxM_{1-x}O_4$ (M=NbV or TaV): Solid Solution Behavior and Second-Harmonic Generating Properties, *J. Solid State Chem.*, 2001, **161**(1), 57–62, DOI: **10.1006/jssc.2001.9266**.

37 A. Michelet, G. Perez, J. Etienne and M. Darriet-Duale, Sur Une Nouvelle Famille De Combinaisons Des Terres Rares

6620 | *Inorg. Chem. Front.*, 2023, **10**, 6613–6621

This journal is © the Partner Organisations 2023

de Formules Ln_2SiS_5 (Ln = La à Nd) et Ln_2GeS_5 (Ln = La), *C. R. Seances Acad. Sci., Ser. C*, 1971, **271**, 513–515.

38 A. Michelet, M. J. Flahaut and M. G. Chaudron, *C. R. Seances Acad. Sci., Ser. C*, 1969, **269**, 1203–1205.

39 H. Qiao, M. T. Saray, X. Wang, S. Xu, G. Chen, Z. Huang, C. Chen, G. Zhong, Q. Dong, M. Hong, H. Xie, R. Shahbazian-Yassar and L. Hu, Scalable Synthesis of High Entropy Alloy Nanoparticles by Microwave Heating, *ACS Nano*, 2021, **15**(9), 14928–14937, DOI: **10.1021/acsnano.1c05113**.

40 H. Zhou and J. He, Synthesis of the New High Entropy Alloy and Its Application in Energy Conversion and Storage, *Front. Energy Res.*, 2020, **8**, 73, DOI: **10.3389/fenrg.2020.00073**.

41 S. Gao, S. Hao, Z. Huang, Y. Yuan, S. Han, L. Lei, X. Zhang, R. Shahbazian-Yassar and J. Lu, Synthesis of High-Entropy Alloy Nanoparticles on Supports by the Fast Moving Bed Pyrolysis, *Nat. Commun.*, 2020, **11**(1), 2016, DOI: **10.1038/s41467-020-15934-1**.

42 Y. Nakahira, S. Shimono, Y. Goto, A. Miura, C. Moriyoshi and Y. Mizuguchi, Synthesis and Characterization of High-Entropy-Alloy-Type Layered Telluride MBi_2Te_4 (M = Ag, In, Sn, Pb, Bi), *Materials*, 2022, **15**(7), 2614, DOI: **10.3390/ma15072614**.

43 S. J. Lee, G. Akopov, A. N. Adeyemi, E. Soto, K. Wu and K. Kovnir, $IrSi_3As_3$: A First Transition Metal Arsenide Non-Linear Optical Material, *J. Mater. Chem. A*, 2023, **11**(22), 11767–11772, DOI: **10.1039/D2TA09313H**.

44 S. Zenkin, A. Gaydaychuk, A. Mitulinsky and S. Linnik, Tailoring of Optical, Mechanical and Surface Properties of High-Entropy Hf-Zr-Ce-Y-O Ceramic Thin Films Prepared by HiPIMS Sputtering, *Surf. Coat. Technol.*, 2022, **433**, 128164, DOI: **10.1016/j.surfcoat.2022.128164**.

45 C.-Y. He, X.-H. Gao, D.-M. Yu, H.-X. Guo, S.-S. Zhao and G. Liu, Highly Enhanced Thermal Robustness and Photothermal Conversion Efficiency of Solar-Selective Absorbers Enabled by High-Entropy Alloy Nitride MoTaTiCrN Nanofilms, *ACS Appl. Mater. Interfaces*, 2021, **13**(14), 16987–16996, DOI: **10.1021/acsami.0c23011**.

46 R. D. Shannon, Revised Effective Ionic Radii and Systematic Studies of Interatomic Distances in Halides and Chalcogenides, *Acta Crystallogr., Sect. A: Cryst. Phys., Diffr., Theor. Gen. Crystallogr.*, 1976, **32**(5), 751–767, DOI: **10.1107/S0567739476001551**.

47 G. Akopov, J. Mark, G. Viswanathan, S. J. Lee, B. C. McBride, J. Won, F. A. Perras, A. L. Paterson, B. Yuan, S. Sen, A. N. Adeyemi, F. Zhang, C.-Z. Wang, K.-M. Ho, G. J. Miller and K. Kovnir, Third Time's the Charm: Intricate Non-Centrosymmetric Polymorphism in $LnSiP_3$ (Ln = La and Ce) Induced by Distortions of Phosphorus Square Layers, *Dalton Trans.*, 2021, **50**(19), 6463–6476, DOI: **10.1039/D1DT00845E**.

48 G. Akopov, G. Viswanathan and K. Kovnir, Synthesis, Crystal and Electronic Structure of La_2SiP_4, *Z. Anorg. Allg. Chem.*, 2021, **647**(2–3), 91–97, DOI: **10.1002/zaac.202000378**.

49 S. Lee, S. L. Carnahan, G. Akopov, P. Yox, L. Wang, A. J. Rossini, K. Wu and K. Kovnir, Noncentrosymmetric Tetrel Pnictides $RuSi_4P_4$ and $IrSi_3P_3$: Nonlinear Optical Materials with Outstanding Laser Damage Threshold, *Adv. Funct. Mater.*, 2021, **31**(16), 2010293, DOI: **10.1002/adfm.202010293**.

50 S. J. Lee, J. Won, L. Wang, D. Jing, C. P. Harmer, J. Mark, G. Akopov and K. Kovnir, New Noncentrosymmetric Tetrel Pnictides Composed of Square–Planar Gold(ı) with Peculiar Bonding, *Chem. – Eur. J.*, 2021, **27**(26), 7383–7390, DOI: **10.1002/chem.202005312**.

This journal is © the Partner Organisations 2023

Inorg. Chem. Front., 2023, **10**, 6613–6621 | **6621**